International Journal of Mass Spectrometry 295 (2010) 72–77

Contents lists available at ScienceDirect

International Journal of Mass Spectrometry

journal homepage: www.elsevier.com/locate/ijms

Improved peak analysis of signals based on counting systems: Illustrated for proton-transfer-reaction time-of-flight mass spectrometry

Thorsten Titzmann[a,b], Martin Graus[b,1], Markus Müller[b,2], Armin Hansel[a,b,*], Alexander Ostermann[c]

[a] Ionimed Analytik GmbH, Technikerstrasse 21a, A-6020 Innsbruck, Austria
[b] Institute of Ion Physics and Applied Physics, University of Innsbruck, Technikerstrasse 25, A-6020 Innsbruck, Austria
[c] Department of Mathematics, University of Innsbruck, Technikerstrasse 13, A-6020 Innsbruck, Austria

ARTICLE INFO

Article history:
Received 28 May 2010
Received in revised form 24 June 2010
Accepted 9 July 2010
Available online 16 July 2010

Counting system
Peak analysis
Dead-time
PTR-TOF

ABSTRACT

Statistical analysis of measured signals from counting systems is a common method to increase the accuracy and precision of peak position and peak area. The most common approach to analyze data gained from counting systems is to fit the data peak by peak using an appropriate probability density function (PDF) like a Gaussian function. Since a counting system creates histograms, the counted data do not represent data points of the anticipated PDF. Therefore, one should not fit any PDF directly to the histogram data. Here we present a solution to this problem by fitting distributions instead of densities. A simple formula allows to correct for Poisson statistics and dead-time effects. The improved peak analysis method is applied to mass spectra obtained from a recently developed proton-transfer-reaction time-of-flight mass spectrometer (PTR-TOF) enhancing the mass accuracy and peak quantification.

1. Introduction

The statistical information provided by a high number of repeated measurements (counting identical particles) is used to get peak position accuracies that are better than those reflected by the difference between two measured points. A widely used method is to fit a probability density function (PDF) to each peak. The expected value of this PDF is interpreted as the peak position. This is the common approach to analyze data gained from counting systems (e.g. [1–6]). However, this method is incorrect and gives wrong results. In Section 5 of this paper we present a correct method to analyze peaks of histograms and show the influences on peak areas and peak positions.

To get accurate results, the data have to be corrected for Poisson statistics and dead time effects. In Section 4 we give a summary of these aspects including the detailed derivations of the associated correction formulas. It should be easy to adopt each of them for other applications than PTR-TOF mass spectrometry. Although the results of this work are useful for any analysis of histogram-data derived from counting systems, we use the terminology of the time-of-flight mass spectrometry. In order to prevent misunderstandings and make it easy to determine which aspects apply to other systems we briefly describe the PTR-TOF.

2. Nomenclature

- The time-of-flight (TOF, flight time) of an ion is the time between the triggered ion extraction and the ion's detection.
- The time-of-flight axis is divided into equidistant intervals. The interval in which an ion is detected is referred to as (time) bin. The bin width is the temporal resolution of the time-to-digital converter.
- Co-arriving ions are ions which arrive within the same bin at the detector. The counting system that has been described has 1 bit resolution and is therefore prone to miscounting whenever co-arriving ions are expected. Co-arriving ions are also present for small average counting rates much lower than one ion per extraction.

3. Instrument and experiments

The PTR mass spectrometry is a widely used technique for online monitoring of volatile organic compounds [7,8]. The PTR-TOF provides the possibility of measuring very low concentrations (pptv level) of volatile organic compounds with a high mass accuracy (a few ppm). The presented research is based on the need for accurate data analysis to take advantage of the PTR-TOF potential. Since

* Corresponding author at: Institute of Ion Physics and Applied Physics, University of Innsbruck, Technikerstrasse 25, A-6020 Innsbruck, Austria
E-mail addresses: thorsten.titzmann@uibk.ac.at (T. Titzmann), martin.graus@noaa.gov (M. Graus), armin.hansel@uibk.ac.at (A. Hansel).
[1] Current address: Chemical Sciences Division, NOAA Earth System Research Laboratory, Boulder, CO, USA.
[2] Current address: CNRS, INSU, UMR5256, IRCELYON, Institut de recherches sur la catalyse et l'environnement de Lyon, Villeurbanne 69626, France.

1387-3806/$ – see front matter © 2010 Elsevier B.V. All rights reserved.
doi:10.1016/j.ijms.2010.07.009

the PTR-TOF is well described in the literature [9,10], only a short description is given here.

The PTR-TOF instrument is an orthogonal acceleration reflectron TOF mass spectrometer (Tofwerk) with a PTR ionization source. The PTR hollow cathode ion source and the corresponding drift tube section (e.g. [11]) produce a continuous beam of ions. This ion beam is collimated by an Einzel lens system and transferred into the accelerator of the TOF mass spectrometer. The accelerator extracts ions into the field-free region with a constant frequency in the range of tens of kHz. The ions are reflected one or three times by the reflectrons before they reach the detector. A time-to-digital converter (TDC) coupled with a constant fraction discriminator (CFD) and a microchannel plate detector (MCP) counts the ions. Since the TDC works on a one-bit and one-channel basis, the recorded spectra for individual extractions show mostly 0 and occasionally 1 ion per time bin. Thousands of these extractions are summarized to give one histogram. These histograms are saved as single spectra per time interval (typically between 0.1 s and 1 min). An arbitrary number of such spectra can be collected to record time series of concentrations. PTR-TOF applications are flux measurements [12], breath gas analysis [1], detection of solid high explosives [13], organic aerosol research [14] and many others.

For this work we used real data from PTR-TOF measurements and simulated data for demonstration purposes. The simulated data was used to compare results with the real values of the underlying ion flight time distributions. These real values are not known for measured data. Additionally the simulated data is used to demonstrate the principles of the presented data analysis methods and make the results easy visible in graphics.

4. Poisson statistics and dead times

Poisson statistics and dead times affect every counting system. Both can cause considerable distortions of peaks in a spectrum. The resulting adverse effects have been well described in the literature of the last decades but most of the corresponding publications focus on nuclear particle detection (e.g. [15,16]). Some of the newer articles are related to non-Poisson processes and dead time issues (e.g. [17,18]) demonstrating the lasting interest in dead time corrections. A correction for Poisson statistics and one type of dead time effects is presented in [19]. Gedcke presented a easy applicable function to correct for both types of dead time effects in time-of-flight mass spectrometry (without derivation or Poisson statistics) [20]. We are describing the relevant aspects of Poisson statistics, extending dead time effects and non-extending dead time effects for our purposes. The result is a simple function that is directly applicable to the measured data for correction of all effects described here.

4.1. Poisson statistics

The number of ions taken from a continuous beam that are detected within a given period of time is subject to variations described by Poisson statistics. The number of co-arriving ions that are available in a single extraction is Poisson distributed with parameter λ. This parameter represents the real average rate of such ions available in the extractor. The probability of having k co-arriving ions available for one extraction is given by the probability density function of the Poisson distribution:

$$P(k) = \frac{\lambda^k}{k!} e^{-\lambda} \tag{1}$$

Since the detector can only distinguish between either 0 or at least 1 ion, the value μ for the measured number of co-arriving ions is given by:

$$\mu = F(\infty) - F(0) = 1 - P(0) = 1 - e^{-\lambda} \tag{2a}$$

where

$$F(n) = \sum_{k=0}^{n} P(k) = e^{-\lambda} \sum_{k=0}^{n} \frac{\lambda^k}{k!} \tag{2b}$$

By solving Eq. (2a) for λ we deduct the real counting rate, λ, corrected for Poisson statistics (but not yet corrected for dead time effects) from the measured counting rate, μ, by:

$$\lambda = -\ln(1 - \mu) \tag{2c}$$

Since a single spectrum (=one extraction recorded by a TDC) shows either 1 or 0 ions in each bin, the statistics cannot be applied to a single extraction. Therefore, histograms are built by summing up series of extractions. The measured counting rate μ is then given by the number of detected ions m divided by the number of extractions r. And the number of ions that have really been extracted n for one bin of this histogram is given by:

$$n = -r \ln\left(1 - \frac{m}{r}\right) \tag{3}$$

This formula corrects the effects of co-arriving ions using the Poisson statistics.

4.2. Dead-times

Whereas co-arriving ions affect only the count rate for the bin in which they reach the detector, dead times impair the correct detection of ions for a lot of bins just after a counting event. Dead time windows are caused by finite response times of MCP and CFD resulting in pulses that are considerably broader than one bin width. All bins inside these pulses are blinded out by an arriving ion. By definition of the dead time, counting systems are not capable of detecting more than one ion during a dead time event.

4.2.1. Non-extending dead time

The TDC sampling rate induces a dead time similar to the CFD pulse. Both dead times are not extended by any further ion arriving within the dead time window, hence the name non-extending dead time (NEDT). The first ion leading to a detector pulse after the NEDT is the next ion which is counted. Both, TDC and CFD have an NEDT. The larger one determines the resulting length of the NEDT window.

During an extraction it is not possible to detect a second ion inside the dead time window. Therefore, the number of extractions for each bin within this dead time interval has to be reduced by one to get the number of "contributing extractions". For convenience we use the term "contributing extractions" for extractions to be considered to potentially contribute to the determination of the counting rate of the ith bin. The number of contributing extractions for one bin equals the number of performed extractions reduced by the number of ions counted inside the dead time window before this bin. Thus the formula that corrects for co-arriving ions and NEDT is given by:

$$n_i = -r \ln\left(1 - \frac{m_i}{s_i}\right), \tag{4}$$

where the index i specifies the ith time bin and s_i denotes the number of contributing extractions of bin i:

$$s_i = r - \sum_{j=i-\vartheta_{ne}}^{i-1} m_j, \ \vartheta < i, \tag{5a}$$

where ϑ_{ne} denotes the NEDT in number of bins.

The sum in Eq. (5a) equals the number of ions registered within the dead time window before bin *i*. When combining it with the extending dead time this formula has to be rearranged:

$$s_i = r\left(1 - \sum_{j=i-\vartheta_{ne}}^{i-1} \frac{m_j}{r}\right) \tag{5b}$$

4.2.2. Extending dead time

The MCP also features a dead time since MCP-pulses have a non-zero width. Similar to the NEDT the MCP dead time inhibits the counting of an ion within the dead time window initiated by the arrival of an ion in one of the preceding bins. In contrast to the NEDT, the MCP dead time window is extended by every further ion arriving at the detector inside the dead time window, hence the name extending dead time (EDT). Therefore it is necessary to take the real λ_i into account.

Derivation of the EDT correction:

Let EDT be 1 ($\vartheta_e = 1$ bin). An ion can only be counted in bin *i*, if no ion was present in bin $i-1$. The probability for this condition is given by $P_{i-1}(0)$. So the number of contributing extractions is given by:

$$s_i = r \cdot P_{i-1}(0) \tag{6a}$$

With $\vartheta_e = 2$ we get:

$$s_i = r \cdot P_{i-1}(0) P_{i-2}(0) \tag{6b}$$

as number of contributing extractions (no ion arrives in the previous two bins).

For any given ϑ_e it then follows:

$$s_i = r \prod_{j=i-\vartheta_e}^{i-1} P_j(0) \tag{6c}$$

Using $P_j(0) = e^{-\lambda_j}$, $\lambda_j = n_j / r$ gives the corrected number of contributing extractions for the *i*th bin:

$$s_i = r \exp\left(-\sum_{j=i-\vartheta_e}^{i-1} \frac{n_j}{r}\right) \tag{7}$$

4.3. Dead time and Poisson correction

Combination of EDT and NEDT for the number of contributing extractions gives:

$$s_i = r\left(1 - \sum_{j=i-\vartheta_{ne}}^{i-1-\vartheta_e} \frac{m_j}{r}\right) \exp\left(-\sum_{j=i-\vartheta_e}^{i-1} \frac{n_j}{r}\right) \tag{8}$$

We eventually get the formula to correct spectra for Poisson statistics, EDT and NEDT by inserting Eq. (8) in Eq. (3):

$$n_i = -rln\left(1 - \left(\frac{m_i}{r}\left(1 - \sum_{j=i-\vartheta_{ne}}^{i-1-\vartheta_e} \frac{m_j}{r}\right)^{-1} \exp\left(\sum_{j=i-\vartheta_e}^{i-1} \frac{n_j}{r}\right)\right)\right) \tag{9}$$

Note that this assumes that all λ_i are constant during *r* extractions. The histogram summed up over *r* extractions can be turned into corrected spectra by applying Eq. (9) to each bin from left to right ($i = 0, 1, 2, \ldots$). The period for a single extraction times the number of extractions, *r*, is the acquisition time for one spectrum. On the one hand, the acquisition time should be chosen to have enough extractions to guarantee statistical behavior and on the other hand to be short enough to have constant λ_i. The effects of these corrections depend strongly on the signal intensity. This is demonstrated in Fig. 1. Signal intensity means 'ions per bin per extraction' in this context. The intensity of the correction is not only influenced by the concentrations but also by the peak width and the bin width. Therefore, no simple relation between concentrations and correction effects can be evaluated. For example:

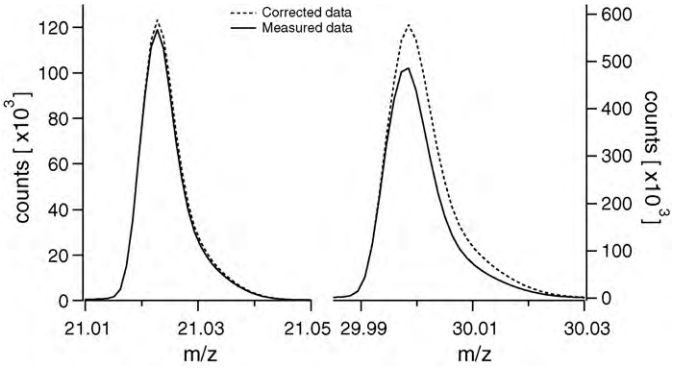

Fig. 1. Effects of the Poisson and dead time corrections. Both peaks are taken from the same PTR-TOF-spectrum which was recorded over 6 min (12×10^6 extractions). The correction for dead time and Poisson effects was done on the 1 s single spectra, each of them based on 33,000 extractions. One second is short enough to assume constant λ_i and the number of extractions is high enough to presume statistical behavior. The more intense peak at $m/z = 30$ causes a relatively stronger correction effect.

(a) Doubling the bin width results in a doubling of the ions per bin ratio.
(b) A change of the instrument settings which decreases the peak width would increase the number of ions per bin.
(c) Peaks at lower m/z ratios cover fewer bins and show more ions per bin than similar peaks at high m/z ratios.

In all these cases the concentration of the ions does not change but the 'ions per bin per extraction' ratio and the effects of the correction increase.

For low intensity peaks the direct effects of these corrections may be very small. If one of the more intense peaks of a spectrum is used uncorrected for calibration purposes (e.g., the mass axis), the introduced error would of course affect all other peaks. For example the exact m/z of the corrected and the not correct peak at $m/z = 21$ differ by 4 ppm and the corrected peak shows 4.37% more counts.

5. Improved peak analysis

We define the relative mass deviation (RMD) as:

$$\mathrm{RMD} = \frac{m - a}{m} \tag{10}$$

where *m* denotes the exact mass calculated from the atomic composition of an ion and *a* denotes the respective measured mass. The maximal RMD in a mass spectra data set is often interpreted as the mass accuracy and is given in units of parts per million (ppm). If one determines the peak position from the measured data without any additional analysis (e.g., choosing the position of the maximum as the peak position) the remaining uncertainty of this position is up to ±0.5 bins. Table 1 illustrates the relative mass deviation across the mass scale assuming a typical flight times of 30 μs for $m/z = 300$ ions, a bin width of 200 ps and a deviation of 0.5 bins.

Table 1
Relative mass deviation of the measured data for 0.5 bins uncertainty (bin width = 200 ps, TOF = 30 μs at m/z = 300).

m/z	20	50	100	200	300
RMD [ppm]	27	17	12	8	7

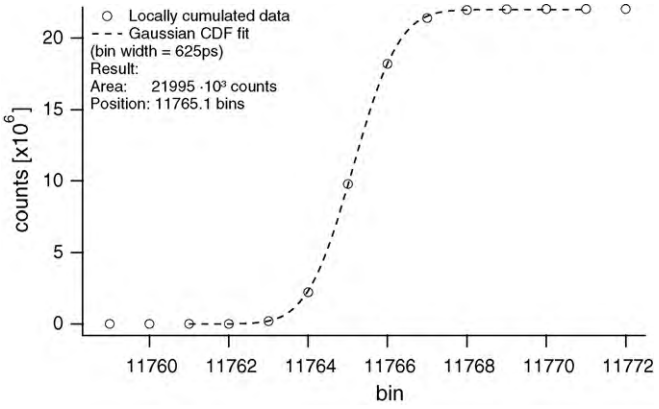

Fig. 2. Cumulated data and Gaussian CDF fit. The data represent one peak. After locally cumulating the data a distribution function is fitted. The data points of the cumulated peak are nodes of the distribution. The original (not cumulated) data are shown in Fig. 3. *Note*: The *Area*-parameter for the CDF equals its maximum.

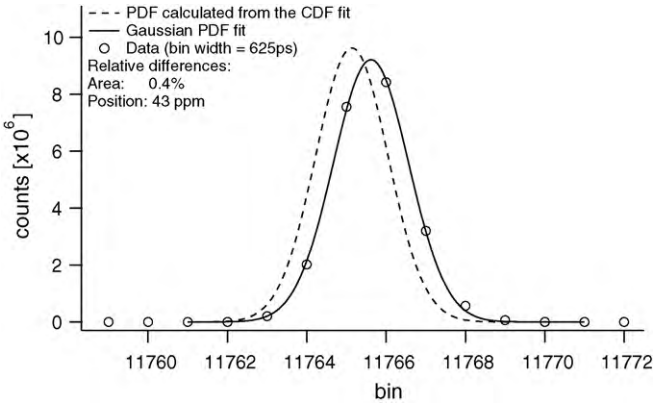

Fig. 3. PDF of a conventional fit and the cumulative fit. The dashed PDF is calculated from the CDF in Fig. 2. The continuous line shows a PDF directly fitted to the data. Significant differences in peak position (43 ppm) and area (0.4%) are observed.

A high-resolution TOF spectrum with reasonably well shaped, intense peaks, however, often allows us to measure peak centers with relative deviations of a few ppm by means of statistical methods. In high-resolution mass spectrometry it is common to use peak-fit routines to achieve such results. We will show that interpreting peaks in TOF spectra as nodes of probability density functions (PDFs) is mathematically incorrect and we are presenting a correct and more robust alternative method.

5.1. Fitting distributions instead of densities

The ith data point of the spectrum represents the number of ions which arrived within the ith time bin. Let t be the bin width, thus each ion arriving in the (left-open) time interval $((i-1)t,\ it]$ counts for the ith data point. Using this data point as a node for a PDF fit is like assuming that each ion counted at the ith data point arrived exactly at time it. For obvious reasons, fitting the data this way may lead to wrong estimates for both the area and the expected value of the arrival time. One can solve this problem by cumulating the data piecewise, bin by bin and peak by peak. Cumulating the data this way gives the correct nodes for a cumulative distribution function (CDF). A PDF may be calculated from the CDF, if necessary.

All fits presented below are done by approximating the data using a least-squares-algorithm. The parameters for the Gaussian functions are *Area*, μ and σ. *Area* denotes the number of ions per peak. This is the area of a PDF, but the maximum of a CDF. The starting values for the approximations are determined from the measured data or set equal the parameters of the simulation.

We determine the starting values from the measured data by *Area* = number of counts, μ = the value where the measured data have their maximum, and σ = FWHM / 2.35 where FWHM is the full width at half maximum of a peak. The FWHM can roughly be estimated from the measured data and this gives sufficiently good starting values.

To demonstrate the impact of using the valid model (CDF) as opposed to the flawed approach (PDF) for measured data, we show spectra with 625 ps bin with and simple Gaussian fits, so the variations between the two methods are easily visible. The result of cumulating one peak and applying the CDF fit is presented in Fig. 2.

Differentiating this CDF will give the corresponding PDF for the ion arrival distribution. Fig. 3 shows the PDFs resulting from both methods. In this example the expected values of the arrival times differ by 43 ppm and the evaluated areas differ by 0.4%. *Note*: The variation in mass accuracy is twice the variation in time-of-flight.

From a measured peak the underlying PDF cannot be determined with absolute certainty. Therefore we simulated data to demonstrate the variations between the two methods.

Gaussian distributed arrival times with parameters *Area* = 20, 000, $\mu = 42$ and $\sigma = 3$ have been used as a shared data base for all of the simulations below. The simulated data points are equidistantly spaced in time (arbitrary time units) and the bin width is assumed to be 10 time units. For data set A we assume the right edge of the bins at time units 10, 20, 30 and so forth, the bin edges for data set B are shifted two time units to the left relatively to data set A (8, 18, 28,. . .). No noise was applied to the simulated data, making the fits straight forward.

Fig. 4 shows the different results of conventional fits of these two data sets. The known parameters of the simulation were used as starting values for the approximation. A valid model, applied to data sets A and B, respectively, should produce identical and correct results. However, the small change in bin positions leads to a non-negligible difference in the fitted PDF. The cumulative fits, however, give correct results for both data sets.

Furthermore the CDF fit method is less affected by higher bin widths than the conventional PDF fit. Based on the simulated data a second pair of data sets was produced with a bin width of 15 time units. The right edge of the first bin of dataset A is located at time

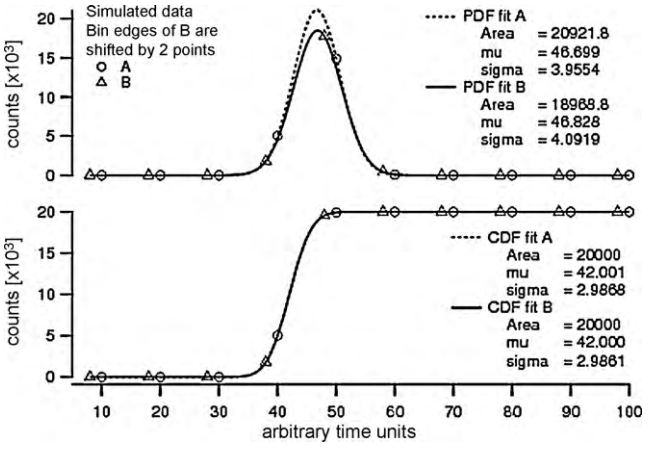

Fig. 4. Simulated data and the resulting fits for different bin positions. Data sets A and B are taken from the same simulation based on a normally distributed data set with parameters *Area* = 20, 000, $\mu = 42$ and $\sigma = 3$. The positions of the bin edges of data set B were shifted by two time units. Fitting one of the data sets should produce the same result for each of them. The conventional PDF fit shows significant differences between the two fits, whereas the results of the CDF fits are really close to each other. Note that the CDF fit of data set A is masked by the CDF fit of data set B.

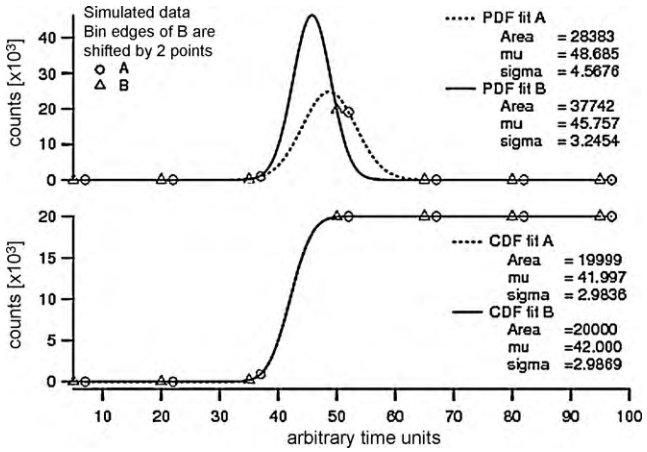

Fig. 5. Problems of conventional fits at high bin widths. The data is based on the simulation used for the data in Fig. 4 (normally distributed with $Area = 20,000$, $\mu = 42$ and $\sigma = 3$). But bin widths for both data sets have been extended to 15 time units. The differences between the conventional fits have dramatically increased. The CDF fits give still good results and match the parameters of the simulation.

unit 7, and at time unit 5 for data set B, respectively. Additionally we changed the starting value of σ to 4 (instead of 3), since deriving the best starting values for the fits from the measured data is not always an easy task, in particular when noise or jitter affects the data. The other starting values for the fits were the same. For data set A (Fig. 5) the variation of TOF is 0.668 bins in this example. Using other starting values, one can also produce a peak having its centroid on the right side of the measured maximum.

Fewer data points per peak or not perfectly chosen starting values may produce really faulty results with the conventional method, whereas the CDF method is more stable with respect to perturbations in the data.

The differences obtained between fitting a PDF or a CDF depend on the number of data points per peak, they decrease with an increasing number of points.[1] In most cases the methodical errors of the conventional PDF fits are reduced by adjusting areas to the number of measured counts or using calibration data to get good peak positions. The average shift of the position (approximately 0.5 bins, particularly for small bin widths) might be corrected, however the additional variation of the estimated peak position cannot be corrected and may contribute in different amounts or directions. Furthermore, applying a faulty approach and reducing the induced errors afterwards is not a good procedure.

5.2. Peak shape and bin width

Our TDC (according to [21]) is usually operated with a bin width of 200 ps. As there are more bins per peak compared to the bin width of 625 ps, the influence of the peak shape is stronger and a Gaussian fit is not good enough. For our purposes we used a fitting function consisting of a Gaussian part and a extreme value distribution to account for the non-Gaussian peak shape:

$$\mathrm{PDF}(t) = \theta\left(\delta\mathcal{E}(t) + \mathcal{N}(t)\right) \tag{11a}$$

$$\mathrm{CDF}(t) = \theta\left(\delta\int_{-\infty}^{t}\mathcal{E}(x)dx + \int_{-\infty}^{t}\mathcal{N}(x)dx\right) \tag{11b}$$

[1] This should not be mixed up with the number of 'ions per bin per extraction', which is significant for the effects of the corrections described in Section 4.

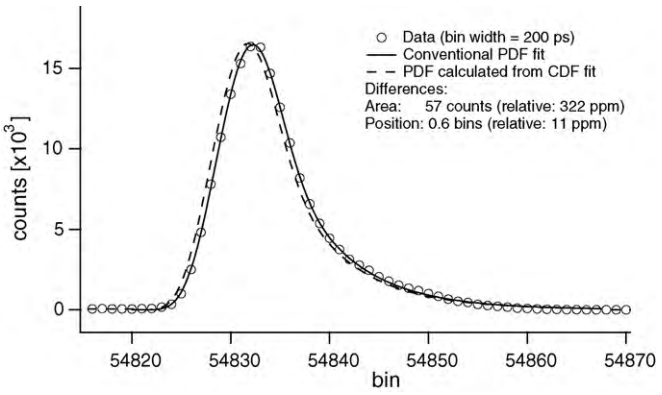

Fig. 6. PDF of a conventional fit and the cumulative fit for data recorded with 200 ps bin width. The better resolution for the peak position gives visible less differences between the both approaches. However, in relation to usually reported mass accuracies of a few ppm the difference is not negligible.

where

$$\mathcal{N}(t) = \frac{1}{\sigma\sqrt{2\pi}}\exp\left(-\frac{(t-\mu)^2}{2\sigma^2}\right)$$

$$\mathcal{E}(t) = \begin{cases} 0 & , t \le \mu - \eta \\ \alpha\,\eta^{\alpha}(t-\mu+\eta)^{-\alpha-1}\exp\left(-\left(\dfrac{t-\mu-\eta}{\eta}\right)^{-\alpha}\right) & , t > \mu - \eta \end{cases}$$

The free parameters for these functions are θ, δ, μ, σ, η and α. The *Area* is given by $Area = \theta\left(\delta + 1\right)$, α has to be greater than 0.

Fig. 6 shows this adapted function. The variation between the conventional fit and the CDF method is visibly smaller for data with higher time resolution than for data recorded with 625 ps bin width. Nevertheless, the difference between the derived flight times in this example is still 11 ppm. This variation is thus at least twice the accuracy normally reached.

6. Summary

In this paper we presented a simple and directly applicable formula to correct for Poisson statistics and all dead time effects in one go. Dead time and Poisson corrections are easy to implement and should be done for every counting system.

Fitting PDFs directly to the measured spectra is not only mathematically incorrect, but the errors may cause considerably worse results with respect to precision and accuracy of both the peak position and the peak intensity. Choosing the incorrect approach does not only affect each individual peak but can also have adverse consequences for whole mass spectra if poorly fitted peaks are used for mass scale calibration purposes. Therefore, all peaks should be fitted by CDF after cumulating them in order to get accurate results. A valid model for estimating the expected value for the peak position must at least be invariant to the relative position of bin edges and the peak maximum. This is the case for the CDF method but not for conventional PDF fits.

Acknowledgments

The author thanks Marc Gonin (TOFWERK) and Alfons Jordan, Gernot Hanel and Stefan Haidacher (IONICON Analytik) for the fruitful discussion of the results of part one. This research has received funding from the Austrian Research Promotion Agency (FFG, Project: 822655).

References

[1] J. Herbig, M. Müller, S. Schallhart, T. Titzmann, M. Graus, A. Hansel, On-line breath analysis with PTR-TOF, Journal of Breath Research 3 (2009) 027004.
[2] H. Junninen, M. Ehn, T. Petäjä, L. Luosujärvi, T. Kotiaho, R. Kostiainen, U. Rohner, M. Gonin, K. Fuhrer, M. Kulmala, A high-resolution mass spectrometer to measure atmospheric ion composition, Atmospheric Measurement Techniques Discussions 3 (2010) 599–636.
[3] M. Kempka, J. Sjödahl, A. Björk, J. Roeraade, Improved method for peak picking in matrix-assisted laser desorption/ionization time-of-flight mass spectrometry, Rapid Communications in Mass Spectrometry (2004) 1208–1212.
[4] J. Meija, J. Caruso, Deconvolution of isobaric interferences in mass spectra, Journal of the American Society for Mass Spectrometry 15 (2004) 654–658.
[5] K. Stamoulis, K. Ioannides, D. Karamanis, Deconvolution of liquid scintillation alpha spectra of mixtures of uranium and radium isotopes, Analytica Chimica Acta (2009).
[6] M. Ward, P. Intallura, C. Natarajan, R. Hadfield, P. Atkinson, Z. Yuan, S. Miki, M. Fujiwara, M. Sasaki, Z. Wang, B. Baek, S. W. Nam, D. A. Ritchie, A. J. Shields, Biexciton cascade in telecommunication wavelength quantum dots, in: Journal of Physics: Conference Series, vol. 210, IOP Publishing (2010), p. 012036.
[7] W. Lindinger, A. Hansel, A. Jordan, On-line monitoring of volatile organic compounds at pptv levels by means of proton transfer-reaction mass spectrometry (PTR-MS) medical applications, food control and environmental research, International Journal of Mass Spectrometry and Ion Processes 173 (1998) 191–241.
[8] J. de Gouw, C. Warneke, Measurements of volatile organic compounds in the earth's atmosphere using proton-transfer-reaction mass spectrometry, Mass Spectrometry Reviews 26 (2007) 223–257.
[9] A. Jordan, S. Haidacher, G. Hanel, E. Hartungen, L. Märk, H. Seehauser, R. Schottkowsky, P. Sulzer, T. Märk, A high resolution and high sensitivity proton-transfer-reaction time-of-flight mass spectrometer (PTR-TOF-MS), International Journal of Mass Spectrometry 286 (2009) 122–128.
[10] M. Graus, M. Müller, A. Hansel, High resolution PTR-TOF: quantification and formula confirmation of VOC in real time, Journal of the American Society for Mass Spectrometry 21 (2010) 1037–1044.
[11] A. Hansel, A. Jordan, R. Holzinger, P. Prazeller, W. Vogel, W. Lindinger, Proton transfer reaction mass spectrometry: online trace gas analysis at the ppb level, International Journal of Mass Spectrometry and Ion Processes 149 (1995) 609–619.
[12] M. Müller, M. Graus, T. Ruuskanen, R. Schnitzhofer, I. Bamberger, L. Kaser, T. Titzmann, L. Hörtnagl, G. Wohlfahrt, T. Karl, First eddy covariance flux measurements by PTRTOF, Atmospheric Measurement Techniques 3 (2010) 387–395.
[13] C. Mayhew, P. Sulzer, F. Petersson, S. Haidacher, A. Jordan, L. Märk, P. Watts, T. Märk, Applications of proton transfer reaction time-of-flight mass spectrometry for the sensitive and rapid real-time detection of solid high explosives, International Journal of Mass Spectrometry 289 (2010) 58–63.
[14] R. Holzinger, A. Kasper-Giebl, M. Staudinger, G. Schauer, T. Röckmann, Analysis of the chemical composition of organic aerosol at the Mt. Sonnblick observatory using a novel high mass resolution thermal-desorption proton-transferreaction mass-spectrometer (hr-TD-PTR-MS), Atmospheric Chemistry and Physics Discussions 10 (2010) 13969–14011.
[15] J. W. Müller, Interval densities for extended dead times, BIMP report 112 (1971).
[16] S. Pommé, Cascades of pile-up and dead time, Applied Radiation and Isotopes (2008) 66.
[17] M. Larsen, A. Kostinski, Simple dead-time corrections for discrete time series of non-Poisson data, Measurement Science and Technology (2009) 20.
[18] R. Willink, On dead-time corrections for estimating rates, Measurement Science and Technology (2010) 21.
[19] T. Stephan, J. Zehnpfenning, A. Benninghoven, Correction of dead time effects in time-of-flight mass spectrometry, Vacuum Science and Technology A 12 (1994) 405–410.
[20] D. A. Gedcke, Dealing with Dead Time Distortion in a Time Digitizer, ORTEC Application Note AN57, 2001.
[21] J. Christiansen, A. Marchioro, F. Moreira, M. Mota, V. Ryjov, S. Debieux, A data driven high performance time to digital converter, in: Proceedings of the 6th Workshop on Electronics for LHC Experiments, Krakow, Poland, 2000.